Optical polarization signatures of black hole X-ray binaries

Vadim Kravtsov [1],[*] Andrei V. Berdyugin,[1] Ilia A. Kosenkov [1], Alexandra Veledina [1,2,3],
Vilppu Piirola,[1] Yasir Abdul Qadir,[1] Svetlana V. Berdyugina,[4] Takeshi Sakanoi,[5] Masato Kagitani[5]
and Juri Poutanen [1,3]

[1] *Department of Physics and Astronomy, University of Turku, FI-20014 Turku, Finland*
[2] *Nordita, KTH Royal Institute of Technology and Stockholm University, Hannes Alfvéns väg 12, SE-10691 Stockholm, Sweden*
[3] *Space Research Institute of the Russian Academy of Sciences, Profsoyuznaya Str. 84/32, Moscow 117997, Russia*
[4] *Leibniz-Institut für Sonnenphysik, Schöneckstr. 6, D-79104 Freiburg, Germany*
[5] *Graduate School of Sciences, Tohoku University, Aoba-ku, 980-8578 Sendai, Japan*

ABSTRACT

Polarimetry provides an avenue for probing the geometry and physical mechanisms producing optical radiation in many astrophysical objects, including stellar binary systems. We present the results of multiwavelength (BVR) polarimetric studies of a sample of historical black hole X-ray binaries, observed during their outbursts or in the quiescent (or near-quiescent) state. We surveyed both long- and short-period systems, located at different Galactic latitudes. We performed careful analysis of the interstellar polarization in the direction on the sources to reliably estimate the intrinsic source polarization. Intrinsic polarization was found to be small (<0.2 per cent) in sources observed in bright soft states (MAXI J0637$-$430 and 4U 1957$+$115). It was found to be significant in the rising hard state of MAXI J1820$+$070 at the level of $\sim$0.5 per cent and negligible in the decaying hard state and during its failed outbursts, while Swift J1357.2$-$0933 showed its absence in the rising hard state. Three (XTE J1118$+$480, V4641 Sgr, V404 Cyg) sources observed during quiescence show no evidence of significant intrinsic polarization, while MAXI J1820$+$070 is the only black hole X-ray binary which showed substantial (>5 per cent) intrinsic quiescent-state polarization with a blue spectrum. The absence of intrinsic polarization at the optical wavelengths puts constraints on the potential contribution of non-stellar (jet, hot flow, accretion disc) components to the total spectra of black hole X-ray binaries.

Key words: polarization – X-rays: binaries.

1 INTRODUCTION

Accreting stellar-mass black holes in X-ray binaries (BHXRBs) are natural laboratories for studying the interaction between matter and radiation under extreme physical conditions. During periods of violent activity – the outbursts – such systems efficiently convert the gravitational energy into radiation that is observed over a broad range of electromagnetic wavelengths, from radio to X/γ-rays. The outburst radio emission is coming from the jet, while the X-rays are produced by the hot accretion flow or corona. Optical and infrared emission, as evidenced by spectral and timing properties, is a product of a complex interplay between the jet, wind, irradiated disc, and hot accretion flow components (Poutanen & Veledina 2014; Uttley & Casella 2014).

An outburst typically continues for several weeks to months, eventually decaying into a quiescent state, a long period of inactivity. The main components of the system – the companion star, the accretion disc, the inner accretion flow – all may contribute to the optical and infrared emission in the quiescence. The hotspot/line (the point of intersection of the stream of matter from the companion star and the outer parts of the disc, see e.g. McClintock, Horne & Remillard 1995; Froning et al. 2011) and jet (Shahbaz et al. 2013) were also proposed as potential sources of quiescent emission.

Identifying different spectral components and studying their radiative properties are essential for understanding the mechanisms that trigger the outbursts. The contribution of different components to the total spectrum has been studied utilizing a variety of methods, with polarimetry often overlooked and undervalued. Polarization carries information about the geometrical properties of the emitting/scattering media, which may otherwise be inaccessible to an observer.

Polarized radiation can be produced by several physical processes, including synchrotron radiation in the presence of an ordered magnetic field of the jet or hot accretion flow, electron scattering in the accretion disc atmosphere or scattering of the accretion disc radiation in the outflow (jet/wind) by electrons or, in quiescence, by dust. Each component has different polarization characteristics (or no polarization at all), which makes polarimetry an excellent tool for probing the geometry of the source and physical mechanisms responsible for optical radiation in black hole X-ray binaries.

A number of recent studies of polarized optical emission of black hole X-ray binaries were focused on BHXRBs in the outbursts (e.g. Shahbaz et al. 2016; Tanaka et al. 2016; Itoh et al. 2017;

[*] E-mail: vakrau@utu.fi

Table 1. List of observed BHXRBs.

Object	Companion	m_V mag	α	δ	π mas	i deg	P_{orb} h	References
XTE J1118+480	K7 V – M1 V	19.6 ± 0.2^a	$11^h\ 18^m\ 10\overset{s}{.}79$	$+48°\ 02'\ 12\overset{''}{.}32$	0.30 ± 0.40	68 ± 2	4.07841(5)	[1, 2, 9]
Swift J1357.2−0933	M5 V	17.27 ± 0.02^a	$13^h\ 57^m\ 16\overset{s}{.}84$	$-09°\ 32'\ 38\overset{''}{.}79$	–	>70	2.8 ± 0.3	[1, 3]
4U 1957+115	–	$\approx19.0^b$	$19^h\ 59^m\ 24\overset{s}{.}01$	$+11°\ 42'\ 29\overset{''}{.}86$	0.07 ± 0.15	$20 - 70$	9.33(1)	[1, 4, 5, 10]
V404 Cyg	K3 III	$\approx18.7^c$	$20^h\ 24^m\ 03\overset{s}{.}82$	$+33°\ 52'\ 01\overset{''}{.}90$	0.42 ± 0.02	67 ± 3	155.35(2)	[1, 6, 7, 11]
V4641 Sgr	B9 III	$\approx13.5^c$	$18^h\ 19^m\ 21\overset{s}{.}63$	$-25°\ 24'\ 25\overset{''}{.}85$	0.17 ± 0.03	72 ± 4	67.61(2)	[1, 8, 12]
XTE J2012+381	–	21.3 ± 0.1^d	$20^h\ 12^m\ 37\overset{s}{.}76$	$+38°\ 11'\ 00\overset{''}{.}77$	–	–	–	[1]
MAXI J1820+070	K6 IV	–	$18^h\ 20^m\ 21\overset{s}{.}94$	$+07°\ 11'\ 07\overset{''}{.}29$	0.37 ± 0.08	73 ± 6	16.4518(2)	[1, 13, 14, 15]
MAXI J0637−430	–	$\approx16.5^c$	$06^h\ 36^m\ 23\overset{s}{.}59$	$-42°\ 52'\ 04\overset{''}{.}10$	–	–	–	[1]

Notes. References: (1) Gaia Collaboration (2021), (2) Gelino et al. (2006), (3) Corral-Santana et al. (2013), (4) Hakala, Muhli & Dubus (1999), (5) Bayless et al. (2011), (6) Miller-Jones et al. (2009), (7) Khargharia, Froning & Robinson (2010), (8) MacDonald et al. (2014), (9) Torres et al. (2004), (10) Thorstensen (1987), (11) Casares, Charles & Naylor (1992), (12) Orosz et al. (2011), (13) Torres et al. (2020), (14) Poutanen et al. (2022), (15) Mikolajewska et al. (2022).
^{a}StanCam photometry, ^{b}Hakala, Muhli & Charles (2014), ^{c}AAVSO magnitudes, ^{d}Hynes et al. (1999).

Kosenkov et al. 2017; Veledina et al. 2019; Kosenkov et al. 2020). However, only a few attempts to study quiescent polarization have been made to date. Dolan & Tapia (1989) found variable optical polarization of BHXRB 1A 0620−00 and constrained its inclination by modelling the dependence of Stokes parameters on orbital phase. Significant quiescent optical polarization of 1A 0620−00 at the level of $P \approx 3$ per cent was later confirmed (Dubus et al. 2008). Russell et al. (2016) claimed detection of near-infrared quiescent intrinsic polarization of 1A 0620−00 and Swift J1357.2−0933. MAXI J1820+070, observed in near-quiescence after its 2018 outburst, demonstrated a large intrinsic polarization degree exceeding 5 per cent in *B*-band and blue polarization spectra, likely caused by scattering either in the hot accretion flow or by the dusty equatorial wedge (Poutanen et al. 2022). A difference by 45° between polarization angle and the position angle of the jet was interpreted as a signature of a high, more than 40°, misalignment between the orbital angular momentum and the black hole spin (Poutanen et al. 2022). Similar polarization signatures, if found in other sources, could be used to study the statistical distribution of orbital-BH spin misalignment angle, constraining binary evolution and black hole formation scenarios.

In this paper, we present a study of optical (BVR) polarization of a sample of BHXRBs during the outbursts and in the quiescent or near-quiescent states. We surveyed both long- and short-period systems with different spectral classes of the companion star, located at different Galactic latitudes. We put tight constraints on the magnitude of intrinsic polarization for most of the sources with the help of polarimetric observations of the field stars. The properties of intrinsic polarization allowed us to estimate the potential contribution of non-stellar components (jet/hot flow) to the total spectra.

2 DATA ACQUISITION AND REDUCTION

The observations of BHXRBs were carried out with two copies of DIPol-2 polarimeter (Piirola, Berdyugin & Berdyugina 2014) and a single unit of DIPol-UF polarimeter (Piirola et al. 2021). One copy of DIPol-2 is installed at the 60 cm Tohoku T60 telescope, Haleakala Observatory, Hawaii, USA; another was mounted on the 60 cm KVA telescope, Observatorio del Roque de los Muchachos (ORM), La Palma, Spain, and was also used as a visitor instrument at 4.2 m William Herschel Telescope (WHT, ORM) and 2.2 m Univesity of Hawaii telescope (UH88, Mauna Kea, Hawaii, USA). DIPol-UF is a visitor instrument installed at the 2.56 m Nordic Optical Telescope (NOT, ORM).

We have collected the polarimetric data on eight BHXRBs with declination $\delta > -30°$ (constrained by the geography of the telescopes used) and visual magnitude $m_V < 21$ mag, limited by the capabilities of the NOT (see Table 1). These include both short- and long-period systems (P_{orb} from ∼2.8 h to 6.5 d), systems with different spectral classes of companion stars (from B9 III to M5 V), located at broad range of Galactic latitudes (Fig. 1 and Table 1).

XTE J1118+480, Swift J1357.2−0933, 4U 1957+115, and XTE J2012+381 were observed for one night each (DIPol-UF at NOT). MAXI J0637−430 was observed for three nights during its soft state in 2019 November (DIPol-2 at T60). V4641 Sgr was observed for a total of 11 nights: eight nights during its quiescent state (three nights with DIPol-2 at T60 in 2018 and five nights with DIPol-UF at NOT in 2019–2020) and for another three nights during its 2021 failed outburst (DIPol-2 at T60). V404 Cyg was observed for two nights during its quiescent state in 2019 July and 2021 July (DIPol-UF at NOT). MAXI J1820+070 was observed for a total of 10 nights during its failed outbursts in 2019 August and 2020 March (DIPol-2 at T60).

We complement the new measurements with the previously published DIPol-2 and DIPol-UF data. These data include the results of polarimetric observations of V404 Cyg and MAXI J1820+070 during a total of 12 and 65 nights respectively. V404 Cyg was monitored for five nights during its 2015 outburst (DIPol-2 at T60), for another five nights, after the outburst has ended (DIPol-2 at WHT) and for two nights during the quiescent state with DIPol-2 mounted at the UH88 (Kosenkov et al. 2017). MAXI J1820+070 was monitored for 12 nights during the rising hard state (DIPol-2 at T60; Veledina et al. 2019), for 26 and 9 nights during the soft and decaying hard states, respectively (DIPol-2 at T60; Kosenkov et al. 2020), and for 18 nights during the quiescent state (DIPol-UF at NOT; Poutanen et al. 2022).

The only relatively bright source in the sample, V4641 Sgr, was observed using a conventional amplifier, while for fainter targets we used electron-multiplication regime of DIPol-UF, which provides better signal-to-noise ratio under such conditions (for a detailed description of instrument modes, see Piirola et al. 2021; Kosenkov 2021c). In addition to the polarimetry, we were able to perform photometric measurements of XTE J1118+480 and Swift J1357.2−0933 with the StanCam CCD photometer, mounted at the NOT. The photometric observations were made within the same night as the polarimetric measurements (MJD 59326). We also used the public AAVSO light curves to estimate *V*-band magnitudes of V404 Cyg, V4641 Sgr, and MAXI J0637−430. Stellar magnitudes for all targets are given in Table 1.
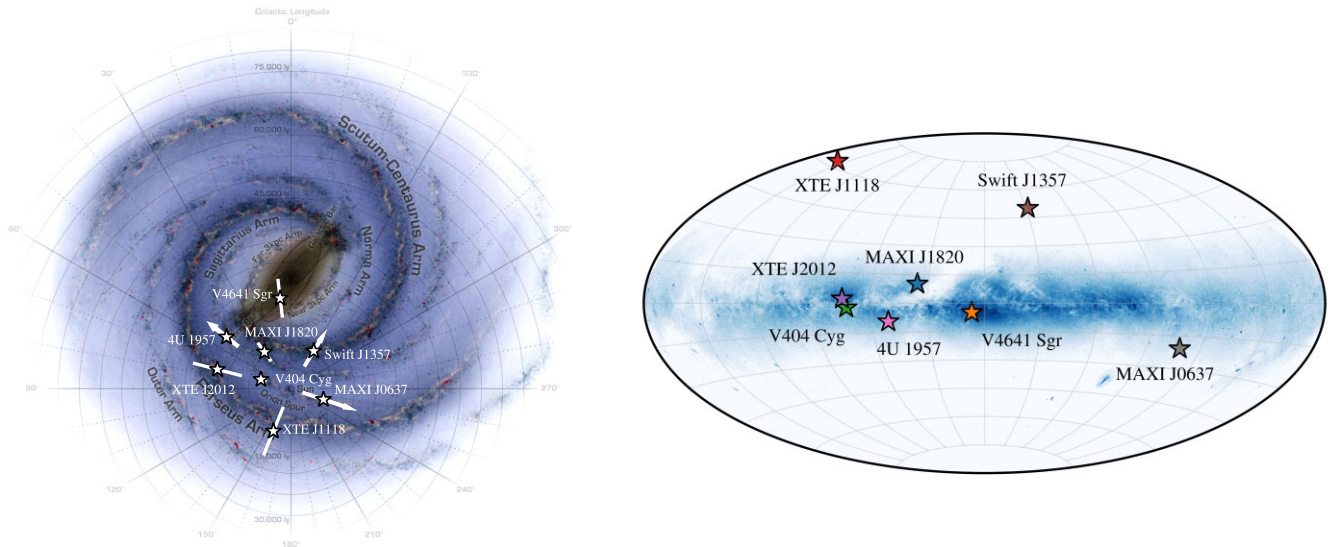
Figure 1. Galactic distribution of the observed X-ray binaries: pole-on view (left-hand panel) and edge-on view (right-hand panel). Background image credit: NASA/JPL-Caltech/R.Hurt (SSC/Caltech), inverted.

Both instruments used for polarimetric observations are remotely operated (Kosenkov 2021a) 'double-image' CCD polarimeters capable of obtaining polarization images in three (BVR) filters simultaneously. The optical beam from a star is split into two orthogonally polarized rays (ordinary 'o' and extraordinary 'e'), resulting in two separate and orthogonally polarized images of a star recorded in different parts of the CCD sensor. The orthogonally polarized images of the sky overlap on each stellar image, effectively eliminating the sky polarization at the instrumental level. The accuracy of polarization measurements can reach 10^{-5}, limited in practice by the photon noise (Piirola 1973; Berdyugin et al. 2018; Piirola et al. 2020).

Each obtained image undergoes standard calibration procedures, including bias and dark subtraction and flat fielding (Berdyugin, Piirola & Poutanen 2019). The difference in brightness between 'o' and 'e' images is measured using differential aperture photometry, and Stokes parameters are computed from their intensity ratios. The individual Stokes parameters are then averaged using '2σ' averaging procedure (Piirola 1975; Kosenkov 2021b, c), obtaining average Stokes parameters and their statistical errors, which are then used to calculate average polarization degree and polarization angle (Simmons & Stewart 1985).

The presence of an interstellar (IS) medium between the observer and the object affects the observed polarization. The IS polarization has to be estimated and subtracted from the observed polarization. One of the most reliable methods for estimating the IS polarization component is to observe a sample of field stars located at distances similar to that of the source. For each source at low galactic latitudes, we observed at least two field stars with close parallaxes, while for the high-latitude objects we used the data from the catalogue of Berdyugin et al. (2014).

3 RESULTS

Results of optical polarization measurements obtained for our sample of BHXRBs are given in Table 2. The results of the determination of their IS polarization are shown in Table 3. The intrinsic polarization estimates are given in Table 4.

3.1 XTE J1118+480

XTE J1118+480 was discovered during its outburst in 2000 by the *Rossi X-ray Timing Explorer* All-Sky Monitor (*RXTE*/ASM; Remillard et al. 2000). The high galactic latitude ($b \approx 62°$) and large distance from the Galactic plane (≈ 1.7 kpc) result in a very small absorption in the direction of the source, making it one of the most popular laboratories for studying outbursts and quiescent states in BHXRBs. The mass of the black hole is estimated to be 6–9 M$_\odot$ (Wagner et al. 2001; Gelino et al. 2006; Chatterjee et al. 2019), while the mass of the companion star is 0.3 ± 0.2 M$_\odot$ (Mirabel et al. 2001). The orbital period of this system is $P_{\rm orb} \approx 4$ h (Torres et al. 2004). The second outburst in 2005 was extensively monitored in different wavelengths from the radio and optical to the X-rays (Pooley 2005; Remillard et al. 2005; Rupen, Dhawan & Mioduszewski 2005; Zurita et al. 2006).

Because of the high galactic latitude, the stellar number density in the direction of XTE J1118+480 is relatively small. As a result, there are no stars located within the instrument field of view (~1 arcmin in the *B*-band and ~45 arcsec in the *V* and *R*-bands). Fortunately, the IS medium density decreases dramatically at high galactic latitudes, making the contribution of the IS polarization component negligible. IS polarization survey of the high galactic latitudes (Berdyugin et al. 2014), puts an upper limit on the IS polarization in the direction of XTE J1118+480 of $P_{\rm IS} < 0.2$ per cent (Table 3 and Fig. 2). To check if the polarization of XTE J1118+480 differs significantly from this value, we first need to correct its observed polarization degree for the bias, which arises due to the small signal-to-noise ratio ($P/\sigma < 5$), shifting the polarization degree towards higher values. The unbiased maximum-likelihood estimator $P_0 = (P^2 - 2\sigma^2)^{1/2}$ from Simmons & Stewart (1985) gives us the following estimations of the true values of the polarization degree: $P_{B,0} = 1.2 \pm 0.8$, $P_{V,0} = 1.4 \pm 0.8$, and $P_{R,0} = 1.3 \pm 0.5$ per cent. Based on these data we can only confirm the absence of substantial (e.g. ≥4 per cent) optical intrinsic polarization in the quiescence for this transient. The previous polarimetric measurement of $P_{\rm obs} = 0.21 \pm 0.16$ per cent in the *V*-band during the outburst in 2000 is consistent with the IS polarization level (Schultz, Hakala & Huovelin 2004).

Table 2. Observed polarization of BHXRBs. Errors are 1σ.

Instrument	State	Date MJD	B P per cent	B θ deg	V P per cent	V θ deg	R P per cent	R θ deg
			B		**V**		**R**	
			P per cent	*θ* deg	*P* per cent	*θ* deg	*P* per cent	*θ* deg
		XTE J1118+480						
DIPol-UF	Quiescence	59326.03	1.65 ± 0.80	22.7 ± 13.0	1.76 ± 0.77	79.4 ± 11.8	1.49 ± 0.53	51.2 ± 9.9
		Swift J1357.2-0933						
DIPol-UF	Failed outburst	59326.10	0.34 ± 0.07	34.5 ± 6.1	0.18 ± 0.08	4.2 ± 12.4	0.25 ± 0.06	69.8 ± 8.5
		4U 1957+115						
DIPol-UF	Soft	59401.14	0.65 ± 0.07	59.4 ± 3.1	0.61 ± 0.09	54.8 ± 4.0	0.62 ± 0.08	60.2 ± 3.9
		V4641 Sgr						
DIPol-2	Quiescence	58347.40	0.46 ± 0.05	34.6 ± 2.9	0.52 ± 0.07	34.8 ± 4.0	0.54 ± 0.07	40.6 ± 3.5
		58348.40	0.41 ± 0.04	44.7 ± 2.8	0.38 ± 0.05	38.7 ± 3.9	0.39 ± 0.04	44.3 ± 2.7
		58351.39	0.42 ± 0.08	33.0 ± 5.0	0.47 ± 0.08	29.8 ± 5.0	0.50 ± 0.09	28.4 ± 5.0
		58686.98	0.53 ± 0.03	43.6 ± 1.6	0.40 ± 0.04	46.0 ± 2.7	0.45 ± 0.02	50.7 ± 0.9
DIPol-UF	Quiescence	58961.19	0.46 ± 0.02	36.8 ± 1.4	0.49 ± 0.06	45.7 ± 3.6	0.42 ± 0.06	48.7 ± 4.3
		58964.21	0.49 ± 0.01	40.2 ± 0.8	0.43 ± 0.03	44.7 ± 1.8	0.44 ± 0.02	50.7 ± 1.0
		58966.22	0.50 ± 0.03	40.1 ± 1.4	0.44 ± 0.04	46.0 ± 2.3	0.48 ± 0.04	50.0 ± 2.4
		58967.20	0.51 ± 0.05	44.4 ± 2.9	0.50 ± 0.10	43.2 ± 5.7	0.45 ± 0.10	51.2 ± 6.1
		59519.71	0.56 ± 0.08	38.5 ± 4.0	0.36 ± 0.15	31.9 ± 10.9	0.29 ± 0.12	46.9 ± 11.2
DIPol-2	Failed outburst	59521.71	0.54 ± 0.08	41.8 ± 4.2	0.37 ± 0.20	45.7 ± 13.9	0.58 ± 0.09	49.5 ± 4.6
		59522.71	0.47 ± 0.08	42.1 ± 4.8	0.48 ± 0.48	38.6 ± 4.4	0.50 ± 0.10	44.4 ± 5.6
		V404 Cyg						
DIPol-2	Rising hard[a]	57195-57200	8.55 ± 0.20	6.7 ± 0.7	7.47 ± 0.06	8.6 ± 0.2	7.51 ± 0.03	6.8 ± 0.1
DIPol-2	Quiescence[a]	57206-57210	7.84 ± 0.16	7.9 ± 0.6	6.58 ± 0.05	11.1 ± 0.2	7.13 ± 0.03	7.7 ± 0.1
DIPol-2	Quiescence[a]	57651-57652	–	–	7.32 ± 0.38	9.7 ± 1.5	7.37 ± 0.21	7.2 ± 0.8
DIPol-UF	Quiescence	58688.02	–	–	8.07 ± 0.41	3.1 ± 1.5	7.30 ± 0.14	5.3 ± 0.5
		59402.16	7.15 ± 0.47	3.6 ± 1.9	7.78 ± 0.21	5.5 ± 0.8	7.85 ± 0.07	6.9 ± 0.3
		MAXI J1820+070						
DIPol-2	Rising hard[b]	58195-58222	0.76 ± 0.01	53.9 ± 0.3	0.79 ± 0.01	54.7 ± 0.4	0.76 ± 0.01	53.3 ± 0.3
		58222-58234	0.76 ± 0.02	51.4 ± 0.6	0.87 ± 0.02	50.5 ± 0.8	0.86 ± 0.02	45.8 ± 0.6
DIPol-2	Soft[c]	58312-58344	0.66 ± 0.01	61.5 ± 0.4	0.67 ± 0.01	62.2 ± 0.5	0.62 ± 0.01	63.5 ± 0.4
DIPol-2	Decaying hard[c]	58406-58428	0.76 ± 0.04	62.2 ± 1.4	0.63 ± 0.06	64.1 ± 2.6	0.67 ± 0.04	62.0 ± 1.7
DIPol-2	Failed outburst	58721-58726	0.67 ± 0.13	65.9 ± 5.6	0.78 ± 0.15	65.0 ± 5.5	0.62 ± 0.10	64.3 ± 4.7
		58911-58932	0.60 ± 0.11	64.5 ± 5.3	0.79 ± 0.20	65.4 ± 7.5	0.71 ± 0.12	68.4 ± 5.0
DIPol-UF	Quiescence[d]	58961-59401	2.88 ± 0.26	-16.8 ± 3.1	1.67 ± 0.25	-13.6 ± 5.5	0.63 ± 0.17	1.5 ± 7.0
		MAXI J0637-430						
DIPol-2	Soft	58792-58796	0.28 ± 0.26	38.8 ± 26.5	–	–	–	–

Notes. Source of the data: [a]Kosenkov et al. (2017), [b]Veledina et al. (2019), [c]Kosenkov et al. (2020), [d]Poutanen et al. (2022).

3.2 Swift J1357.2−0933

The black hole transient Swift J1357.2−0933 was discovered in 2011 using *Neil Gehrels Swift Observatory* Burst Alert Telescope (*Swift*/BAT; Krimm et al. 2011). Similar to XTE J1118+480, the binary separation of Swift J1357.2−0933 is very small (the orbital period $P_{\rm orb} \approx 2.8$ h) and the black hole in the system has a mass $M_{\rm BH} > 9$ M$_\odot$ (Mata Sánchez et al. 2015; Casares 2016). The analysis of optical spectra revealed remarkable broad double-peaked Hα emission line, which is a strong indication of a high ($i > 70°$) binary inclination (Corral-Santana et al. 2013).

During our observations of the source, the beginning of its optical and X-ray re-brightening event was reported (Baglio et al. 2021; Bellm 2021; Beri et al. 2021; Caruso et al. 2021). There are no nearby stars in the field of view of Swift J1357.2−0933, but its location at the high galactic latitude ($\approx 50°$) allows us to put the upper limit of 0.2 per cent on the expected level of IS polarization from the survey of Berdyugin et al. (2014), see Table 3 and

Fig. 2. The small value of the observed polarization of the source is consistent with the IS polarization level and hence the optical polarization of Swift J1357.2−0933 observed during its transition from the quiescence to the faint outburst (with X-ray luminosity of about $L_{\rm X} \sim 10^{34}$ erg s^{-1}; Beri et al. 2021), most likely has an IS origin.

Shahbaz et al. (2003) argued that the quiescent optical to mid-infrared emission is dominated by the synchrotron jet emission. This emission is expected to be strongly (up to 70 per cent) polarized, which allows us to estimate its contribution to the total optical spectrum. Our non-detection of intrinsic polarization at the level of $P_{\rm int} < 0.2$ per cent suggests this contribution to be less than a few per cent of the total optical emission during the initial rise to the outburst. Additional polarization measurements during the true quiescent state are needed to estimate the role of the synchrotron emission to the quiescent optical spectrum of Swift J1357.2−0933.

Table 3. Polarization of field stars.

Field star	Identifier HD/BD/Gaia DR3	Parallax mas	Angular separation	*B* P per cent	*θ* deg	*V* P per cent	*θ* deg	*R* P per cent	*θ* deg
			XTE J1118+480						
Ref A[a]	BD + 48 1955	4.18 ± 0.02	~100 arcmin	–	–	0.06 ± 0.03	89 ± 12	–	–
			Swift J1357.2-0933						
Ref A[a]	HD 122835	4.15 ± 0.30	~100 arcmin	–	–	0.12 ± 0.05	101 ± 13	–	–
			4U 1957+115						
Ref A	4303869526257087360	0.36 ± 0.13	<1 arcmin	0.59 ± 0.15	53 ± 7	0.72 ± 0.12	53 ± 5	0.48 ± 0.08	62 ± 5
Ref B	4303869599285320832	0.17 ± 0.08	<1 arcmin	0.65 ± 0.07	55 ± 3	–	–	0.52 ± 0.05	54 ± 3
			V4641 Sgr						
Ref A	4053096384526868736	0.24 ± 0.03	<10 arcmin	0.56 ± 0.08	55 ± 4	0.40 ± 0.03	50 ± 2	0.39 ± 0.02	56 ± 1
Ref B	4053096491998429952	0.40 ± 0.03	<10 arcmin	0.54 ± 0.05	52 ± 3	0.62 ± 0.08	51 ± 4	0.59 ± 0.06	62 ± 3
Ref C	4053096315807371008	0.51 ± 0.03	<10 arcmin	0.26 ± 0.05	59 ± 5	0.29 ± 0.04	62 ± 4	0.33 ± 0.02	63 ± 2
Ref D	4053096320199414528	0.65 ± 0.03	<10 arcmin	0.57 ± 0.08	67 ± 4	0.45 ± 0.09	65 ± 6	0.45 ± 0.06	74 ± 4
Ref E	4053096595077613568	0.42 ± 0.03	<10 arcmin	0.70 ± 0.11	56 ± 4	0.47 ± 0.07	56 ± 4	0.40 ± 0.02	51 ± 2
Ref F	4053096487606085632	0.53 ± 0.03	<10 arcmin	0.29 ± 0.08	67 ± 8	0.38 ± 0.08	77 ± 6	0.35 ± 0.06	69 ± 5
			V404 Cyg						
Ref 4040[b]	2056188620566335360	0.14 ± 0.11	1.4 arcsec	–	–	6.64 ± 0.22	12 ± 1	7.28 ± 0.09	9 ± 1
Ref 4042[b]	2056188865390747136	0.35 ± 0.04	<10 arcmin	–	–	7.09 ± 0.42	11 ± 2	8.47 ± 0.17	9 ± 1
Ref 4043[b]	2056190136700843264	0.34 ± 0.03	<10 arcmin	6.92 ± 0.29	3 ± 1	5.20 ± 0.15	11 ± 1	6.47 ± 0.07	11 ± 1
			XTE J2012+381						
Ref A	2061667762205170048	0.23 ± 0.05	<1 arcmin	3.36 ± 0.60	88 ± 5	3.90 ± 0.19	84 ± 1	3.69 ± 0.07	83 ± 1
Ref B	2061673435561995008	0.19 ± 0.05	<1 arcmin	2.58 ± 0.42	83 ± 5	3.78 ± 0.16	90 ± 1	3.71 ± 0.07	88 ± 1
			MAXI J1820+070						
Ref 1-5	2,3,6,7,9[c]	0.15 - 0.44	<10 arcmin	0.80 ± 0.03	64 ± 1	0.70 ± 0.03	69 ± 1	0.60 ± 0.02	64 ± 1
			MAXI J0637.430						
Ref A	5569292377717900288	0.67 ± 0.01	<10 arcmin	0.57 ± 0.08	39 ± 4	–	–	–	–
Ref B	5569291931041304960	0.78 ± 0.02	<10 arcmin	0.42 ± 0.08	38 ± 6	–	–	–	–
Ref C	5569291999760781312	1.09 ± 0.26	<10 arcmin	0.14 ± 0.07	67 ± 14	–	–	–	–

Notes. [a]Nearest stars from the catalogue of Berdyugin, Piirola & Teerikorpi (2014).
[b]Reference stars from table 3 of Kosenkov et al. (2017).
[c]Polarization is given as the weighted average of the polarization of five field stars from table 2 of Veledina et al. (2019).

Table 4. Intrinsic polarization measurements of the observed sample. Both detected values and the upper limits are given. Intrinsic polarization estimate for XTE J2012+381 is not reliable, because of the confusion with the foreground star, and is not given in the table.

Source	State	P_B per cent	P_V per cent	P_R per cent
XTE J1118+480	Q	1.2 ± 0.8	1.4 ± 0.8	1.3 ± 0.5
Swift J1357.2−0933	RH[a]	≤0.5	≤0.4	≤0.4
4U 1957+115	S	≤0.2	≤0.3	≤0.3
V4641 Sgr	RH[a]	≤0.1	≤0.1	≤0.1
	Q	≤0.1	≤0.1	≤0.1
V404 Cyg	RH	0.8 ± 0.3	1.1 ± 0.1	0.5 ± 0.1
	Q	≤0.5	≤0.5	≤0.5
MAXI J1820+070	RH1	0.28 ± 0.01	0.36 ± 0.01	0.30 ± 0.01
	RH2	0.34 ± 0.02	0.51 ± 0.02	0.53 ± 0.02
	S	0.16 ± 0.01	0.15 ± 0.01	0.02 ± 0.01
	DH	0.06 ± 0.04	0.13 ± 0.06	0.09 ± 0.04
	RH[a]	≤0.3	≤0.4	≤0.3
	Q	3.2 ± 0.2	1.9 ± 0.2	0.9 ± 0.1
MAXI J0637−430	S	≤0.2	–	–

Notes. [a]Failed outburst. States: Q – quiescence, RH – rising hard, S – soft, DH – decaying hard (see Table 2).

3.3 4U 1957+115

4U 1957+115 was detected by *Uhuru* satellite in 1973 (Giacconi et al. 1974) and since then remains in the soft state. Its emission is dominated by the accretion disc (Wijnands, Miller & van der Klis 2002) and modulated with the orbital period $P_{orb} \approx 9.3$ h in optical light (Thorstensen 1987; Hakala et al. 1999; Bayless et al. 2011; Hakala et al. 2014), while the X-rays show no orbital modulation (Nowak & Wilms 1999). Optical light-curve modelling (Bayless et al. 2011) constrained inclination to be in range of $20° < i < 70°$.

To estimate the IS polarization in the direction of 4U 1957+115, we measured the polarization of two nearby field stars (Table 3 and Fig. 2). The observed degree $P_{obs} = 0.60 \pm 0.08$ per cent and the position angle $\theta_{obs} = 58° \pm 5°$ of linear polarization of 4U 1957+115 coincides with the IS values within the measurement errors.
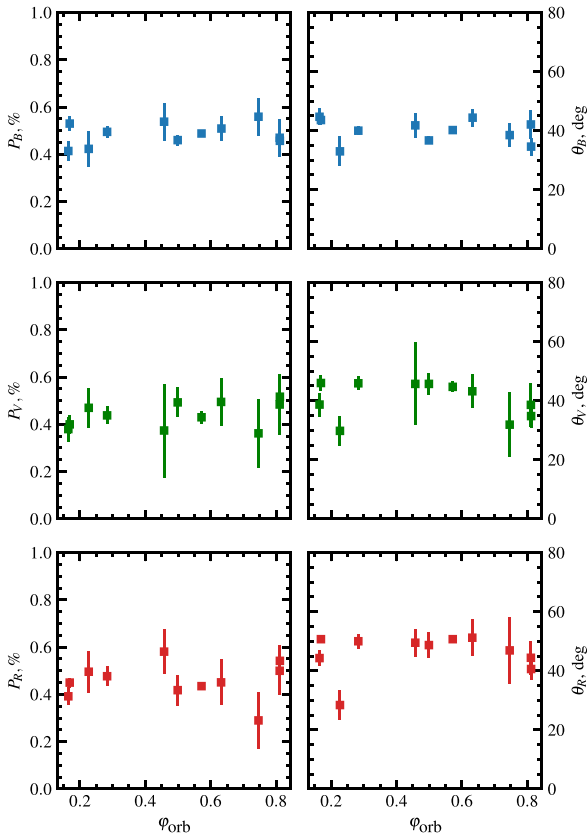
3.4 V4641 Sgr

Intermediate mass X-ray binary and a microquasar V4641 Sgr shows highly atypical behaviour for an X-ray transient. After the decay of the first outburst (in 't Zand et al. 1999), it underwent a series of over ten failed outbursts (full list can be found in Salvesen & Pokawanvit 2020). The compact object was dynamically identified as a black hole with the mass $M_{bh} = 6.4 \pm 0.6$ M$_\odot$, and mass of the companion was found to be $M_c \approx 3$ M$_\odot$ (MacDonald et al. 2014). The relatively high mass of the companion makes V4641 Sgr one of the largest known Roche lobe-filling X-ray binaries. Orbital period of the binary is $P_{orb} \approx 2.817$ d (Orosz et al. 2001) and the inclination of the orbit $i = 72° \pm 4°$ (MacDonald et al. 2014).

We observed the source in 2018 August and 2021 November with DIPol-2, when an increased optical activity of V4641 Sgr with 0.3−0.5 mag enhancement was detected (Kong 2018; Zhirkov et al. 2021). DIPol-UF observations were performed during its quiescent
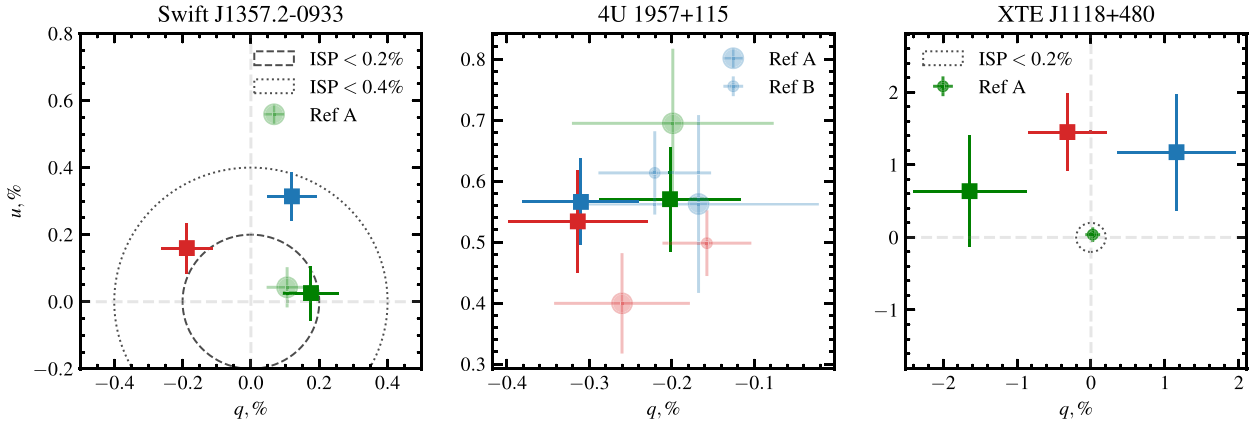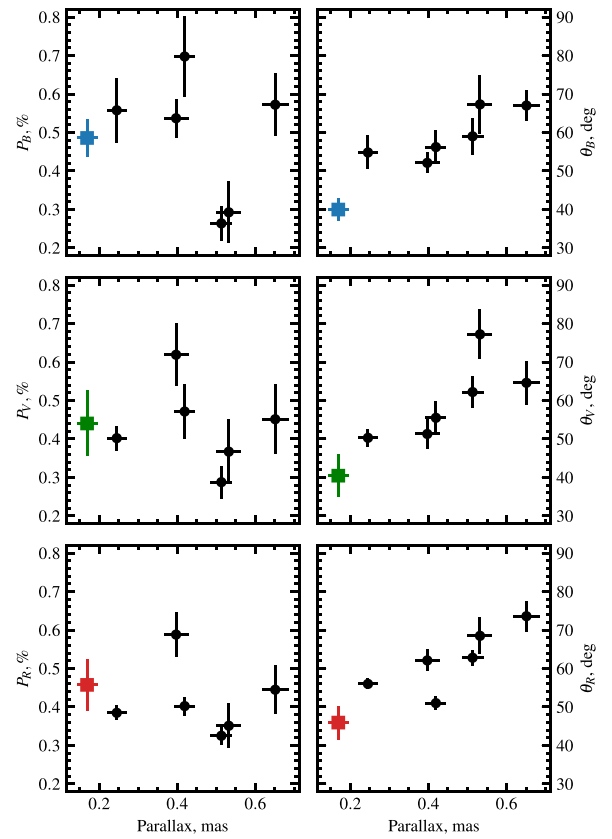
Figure 2. Normalized observed Stokes parameters (q, u) for Swift J1357.2−0933 , 4U 1957+115 , and XTE J1118+480 (from left to the right). The blue, green, and red squares with 1σ errors correspond to the B, V, and R optical polarimetric measurements of the targets and the circles correspond to nearby stars.

Figure 3. Dependence of the observed polarization degree (left-hand column) and polarization angle (right-hand column) of V4641 Sgr on the orbital phase in the BVR bands (from top to bottom). The errors are 1σ. The orbital period $P_{orb} = 2.8173 \pm 0.00001$ d is taken from Orosz et al. (2001).

Figure 4. Dependence of the observed polarization degree (left-hand column) and polarization angle (right-hand column) on parallax for V4641 Sgr (coloured squares) and field stars (black circles) in the BVR bands (from top to bottom).

state. The object shows rather constant level of polarization $P_{obs} = 0.50 \pm 0.05$ per cent with the position angle of $\theta_{obs} \approx 40°$ during the whole monitoring period (see Table 2). To examine the orbital variability, we folded the polarimetric data with the orbital period – the resulting polarization shows no dependence on the orbital phase (Fig. 3). To analyse the behaviour of the IS polarization, we observed six field stars with the parallaxes $\pi = 0.2-0.6$ mas

(Fig. 4). The degree of observed polarization falls in the range of 0.3–0.7 per cent for all observed stars, while the polarization angle increases with the parallax almost linearly. We conclude that the values of average polarization and polarization angle of V4641 Sgr in all passbands are consistent with the IS polarization. This fact, along with the absence of orbital variability of observed polarization,

suggests that V4641 Sgr has no intrinsic optical polarization in either the quiescence or failed outbursts.

3.5 V404 Cyg

Initially discovered as Nova Cyg 1938, V404 Cyg underwent outbursts in 1956 and 1989 (Richter 1989), and two outbursts in 2015 (Barthelmy et al. 2015; Lipunov et al. 2015). Since its first X-ray detection in 1989 by the *Ginga* satellite (Makino et al. 1989), V404 Cyg has been extensively monitored in wide energy ranges, including radio, optical, X-ray and gamma-rays (Casares & Charles 1994; Życki, Done & Smith 1999; Corbel, Koerding & Kaaret 2008; Loh et al. 2016). During the 2015 outburst, V404 Cyg reached 40 Crab in the hard X-rays (Rodriguez et al. 2015) and brightened in the optical from $m_V \approx 18$ up to $m_V \approx 11$ mag (Kimura et al. 2016).

V404 Cyg is one of a few low-mass X-ray binaries (LMXB) with orbital parameters and distance known with great accuracy. The K-type companion with the mass of ~ 1 $M_\odot$ orbits a ~ 9 $M_\odot$ black hole primary with the orbital period of ~ 6.5 d on the orbit, inclined to the observer on $i \approx 67°$ (Khargharia et al. 2010). An accurate parallax $\pi = 0.42 \pm 0.02$ mas has been measured in Miller-Jones et al. (2009).

The 2015 outburst triggered several polarimetric campaigns (e.g. Shahbaz et al. 2016; Tanaka et al. 2016; Itoh et al. 2017; Kosenkov et al. 2017). Optical and near-infrared (ONIR) polarimetric measurements revealed high value of IS polarization (~ 7 per cent, see Table 3 and Tanaka et al. 2016) with atypical wavelength dependence – a potential signature of multiple dust clouds between the source and the observer (Kosenkov et al. 2017). V404 Cyg showed statistically significant intrinsic ONIR polarization during its re-brightening (IS polarization was estimated by observing a sample of field stars, see Table 3 and Kosenkov et al. 2017). Observed shortly after the outburst, however, V404 Cyg demonstrated no intrinsic polarization: its observed polarization was identical to the observed polarization of a visually close ($\sim 1''.4$; Udalski & Kaluzny 1991) star, which was reliably resolved as soon as the brightness of the LMXB dropped to the quiescent level.

Several conditions affect the accuracy of polarimetric measurements of V404 Cyg and surrounding field stars. First, the presence of the visually close companion complicates target separation, especially under poor weather conditions (with seeing $\geq 1''.0$). Secondly, relatively high IS extinction ($A_V \approx 3.5$; Shahbaz et al. 2003), caused by the proximity to the galactic plane, increases the total integration time needed for reliable measurements, especially in the *B* filter. Both new polarimetric measurements of V404 Cyg made with the DIPol-UF suffer from these conditions: the first measurement (made during the technical night allocated for commissioning of DIPol-UF) was too short to reach sufficiently high accuracy in *B* and *V* filters, while the second measurement was carried out when the seeing was poor. Despite these obstacles, the quiescent polarization degree and angle in the *R* filter (where accuracy is adequate) are in agreement with the polarization obtained for the nearest field stars and are consistent with the previous observations (Kosenkov et al. 2017). We therefore see no signs of intrinsic polarization in V404 Cyg during the quiescence.

3.6 MAXI J1820+070

The LMXB MAXI J1820+070 was discovered in March of 2018 with the Monitor of All-sky X-ray Image (MAXI) nova alert system as a bright X-ray source (Kawamuro et al. 2018), which later was associated with the ASASSN-18ey optical transient (Denisenko 2018). Over the following ~ 9 months MAXI J1820+070 underwent a violent outburst, reaching $m_V \approx 11.5$ mag (Littlefield 2018) and

~ 3 Crabs in X-rays (Bozzo et al. 2018). The initial hard state lasted for ~ 4 months and was followed by a soft state, in which the source resided for the same amount of time. MAXI J1820+070 had never reached the true quiescence after the 2018 outburst has ended; instead, it underwent three (Stiele & Kong 2020) nearly identical in profile and duration 'failed' outbursts, each time increasing its optical brightness from $m_V \approx 18.5$ to $m_V \approx 13.5$ mag.

Since the onset of the 2018 outburst, MAXI J1820+070 was extensively monitored both photometrically and polarimetrically. Similar to V404 Cyg, MAXI J1820+070 demonstrated small but statistically significant variable intrinsic optical polarization during rising hard and soft states (Veledina et al. 2019; Kosenkov et al. 2020). The position angle of intrinsic polarization in the rising hard state ($\sim 24°$; Kosenkov et al. 2020) was found to be in good agreement with the position angles of radio (Bright et al. 2018) and X-ray (Espinasse et al. 2020) jets, providing evidence for a connection between the scattering medium and the jet axis.

MAXI J1820+070 showed no significant intrinsic polarization near the peaks of two failed outbursts (Table 2). Its observed polarization remained in good agreement with the IS polarization measured from a sample of field stars. Surprisingly, a dramatically different polarization picture was observed in the (near-)quiescent state: MAXI J1820+070 showed substantially higher (up to 5 per cent in *B*) intrinsic polarization with polarization angles offset from the jet axis (Poutanen et al. 2022). The misalignment and large polarization remained surprisingly stable between failed outbursts, suggesting a strong connection to geometrical properties of the source, which can be probed only during inactive phases, otherwise remaining completely obscured by the accretion–ejection processes happening during outbursts.

3.7 MAXI J0637−430

MAXI J0637−430 was discovered on 2019 November 2 by MAXI X-ray monitor (Negoro et al. 2019). A few hours after the discovery, the optical counterpart with the brightness of $m_u \approx 15$ mag was found in the direction on the X-ray transient with *Swift*/UVOT (Kennea et al. 2019). Follow-up optical spectroscopic (Strader et al. 2019) and X-ray (Tomsick et al. 2019) observations suggested that the source is an LMXB hosting a black hole. The mass of the compact object has not been reliably measured yet (using, e.g. quiescent state spectroscopy), but it was estimated $M_{BH} = 5$–12 $M_\odot$ from the X-ray flux and the distance constraint of $d < 10$ kpc (Jana et al. 2021).

The absence of a reliable estimate of the distance to the object complicates the estimation of IS polarization. To constrain it, we observed three field stars near MAXI J0637−430 with distances in the range of 0.9–1.5 kpc (Table 3). The polarization is higher for more distant sources reaching in the *B*-band about 0.6 per cent. The observed polarization of MAXI J0637−430 (Table 2) is consistent with zero with the 3σ upper limit of 1.1 per cent (obtained with Monte Carlo simulations) and is consistent with the IS values.

3.8 XTE J2012+381

An X-ray transient XTE J2012+381 was discovered in 1998 by *RXTE* (Remillard et al. 1998) reaching 150 mCrab in the 3–20 keV X-ray band. The Karl G. Jansky Very Large Array (VLA; Thompson et al. 1980) observations obtained in the same year revealed a radio source in the direction of the transient (Hjellming, Rupen & Mioduszewski 1998). Optical observations were able to identify a faint ($m_R \approx 20$ mag) optical counterpart at the coordinates, consistent with the radio and X-ray counterparts (Hynes et al. 1999).

The faint optical counterpart of XTE J2012+381 is heavily blended with the visually close ($\sim 1\rlap{.}''1$; Hynes et al. 1999) and much brighter foreground star. We measured the polarization of the binary ($P_B = 0.06 \pm 0.14$, $P_V = 0.12 \pm 0.09$, $P_R = 0.17 \pm 0.07$ per cent), but our observational capacities did not allow us to separate the contribution of XTE J2012+381 from the contribution of the foreground star to the resulting value of linear polarization. Nevertheless, we obtained the polarization of two nearby field stars and estimated the value of IS polarization in the direction to the binary (Table 3), which can be used in the future polarization studies.

4 SUMMARY AND DISCUSSION

We performed optical polarimetric observations of a set of Galactic BHXRBs in various spectral states. Our survey consists of both long- and short-period systems located at low and high Galactic latitudes and residing in quiescent, hard, and soft states. We used observations of the nearby field stars to estimate the IS polarization in the direction of the selected BHXRBs. This allowed us to constrain the intrinsic polarization in these sources. For virtually all systems in our sample, we were able to only put upper limits on the intrinsic polarization – see summary in Table 4.

Optical and infrared emission of BHXRBs consists of the contributions of several components – the companion star, accretion disc, inner accretion flow, hot spot/line, and jet. Their relative role in the total spectrum changes with state. All of them can be polarized, but the polarization degree and its spectral dependence are expected to be different and can be used to discriminate between them.

In the soft state, the optical emission is likely dominated by the disc emission, and the polarization may arise from the scattering processes in its atmosphere. In the case of pure electron scattering (Chandrasekhar 1960; Sobolev 1963), the polarization is expected to increase with the inclination of the disc, reaching a maximum of $P = 11.7$ per cent for the edge-on disc. The observed soft-state sources, 4U 1957+115, MAXI J0637−430, and MAXI J1820+070, on the other hand, show polarization below ~ 1 per cent, albeit the latter having high inclination. This may indicate either the complex structure of the accretion disc, such as warp, or the interplay of the scattering and absorption effects in the atmosphere, both of these effects tend to decrease the total polarization.

Likewise, hard-state sources during both regular and failed outbursts show low levels of intrinsic polarization (<1 per cent). Only MAXI J1820+070 – and only during the rising hard state – has a reliable estimate of intrinsic polarization ($P \sim 0.5$ per cent). Its polarization angle coincides with the position angle of discrete ejections detected in the source and the epochs of polarization detection coincide with the detection of winds in the source (Kosenkov et al. 2020). This, combined with the red polarization spectrum, may indicate that the polarization is produced by scattering in the wind of the seed photons with the red spectrum. Such synchrotron emission is produced either in the hot accretion flow or jet. The absence of significant intrinsic polarization in all hard-state sources in our sample advocates against significant contribution of the jet synchrotron emission itself, as it is expected to be polarized at the level of tens of per cent (Rybicki & Lightman 1979; Veledina et al. 2019).

The detection of a significant, $P_B \sim 5$ per cent, quiescent-state polarization with blue spectrum in MAXI J1820+070 put tight constraints on its origin (Poutanen et al. 2022). Such polarization can be produced by the single Compton scattering in a hot medium, with seed photons coming from the surrounding disc (ring) of a cool matter. At the same time, scattering in the disc itself is excluded based on the high value of the polarization, while polarization of jet synchrotron emission is disfavoured based on its spectrum. In contrast to MAXI J1820+070, the other two quiescent-state binaries in our sample show low levels of polarization, $P \lesssim 1$ per cent. This may indicate the absence of the hot medium in these sources and may indicate that they have entered the true quiescent state (while MAXI J1820+070 is still accreting at a very low level). Future high-precision polarimetric observations of sources in quiescent (and near-quiescent) states are required to confirm the proposed scenario. Confirmation of the presence of the hot accretion flow in sources undergoing frequent outbursts may indicate its connection to the outburst triggers.

DATA AVAILABILITY

The data underlying this article will be shared on reasonable request to the corresponding author.

REFERENCES

Baglio M. C., Caruso E., Russell D. M., Saikia P., Bramich D. M., Lewis F., 2021, Astron. Telegram, 14729, 1

Barthelmy S. D., D'Ai A., D'Avanzo P., Krimm H. A., Lien A. Y., Marshall F. E., Maselli A., Siegel M. H., 2015, GCN Circ., 17929, 1

Bayless A. J., Robinson E. L., Mason P. A., Robertson P., 2011, ApJ, 730, 43

Bellm E. C., 2021, Astron. Telegram, 14539, 1

Berdyugin A., Piirola V., Teerikorpi P., 2014, A&A, 561, A24

Berdyugin A., Veledina A., Kosenkov I., Poutanen J., Tsygankov S., Kajava J. J. E., Kagitani M., Sakanoi T., 2018, Astron. Telegram, 11445, 1

Berdyugin A., Piirola V., Poutanen J., 2019, in Mignani R., Shearer A., Słowikowska A., Zane S., eds, Astrophysics and Space Science Library Vol. 460, Astronomical Polarisation from the Infrared to Gamma Rays. Springer Nature, Cambridge, UK, p. 33

Beri A. et al., 2021, Astron. Telegram, 14573, 1

Bozzo E., Savchenko V., Ferrigno C., Ducci L., Kuulkers E., Ubertini P., Laurent P., 2018, Astron. Telegram, 11478, 1

Bright J., Motta S., Fender R., Perrott Y., Titterington D., 2018, Astron. Telegram, 11827, 1

Caruso E., Russell D. M., Baglio M. C., Saikia P., Bramich D. M., Lewis F., 2021, Astron. Telegram, 14623, 1

Casares J., 2016, ApJ, 822, 99

Casares J., Charles P. A., 1994, MNRAS, 271, L5

Casares J., Charles P. A., Naylor T., 1992, Nature, 355, 614

Chandrasekhar S., 1960, Radiative transfer. Dover Publications, Inc., New York, USA

Chatterjee D., Debnath D., Jana A., Chakrabarti S. K., 2019, Ap&SS, 364, 14

Corbel S., Koerding E., Kaaret P., 2008, MNRAS, 389, 1697

Corral-Santana J. M., Casares J., Muñoz-Darias T., Rodríguez-Gil P., Shahbaz T., Torres M. A. P., Zurita C., Tyndall A. A., 2013, Science, 339, 1048

Denisenko D., 2018, Astron. Telegram, 11400, 1

Dolan J. F., Tapia S., 1989, PASP, 101, 1135

Dubus G., Kern B. D., Chaty S., Foellmi C., 2008, in VII Microquasar Workshop: Microquasars and Beyond. Foca, Izmir, Turkey, p. 115

Espinasse M. et al., 2020, ApJ, 895, L31

Froning C. S. et al., 2011, ApJ, 743, 26

Gaia Collaboration 2021, A&A, 649, A1

Gelino D. M., Balman Ş., Kızıloğlu Ü., Yılmaz A., Kalemci E., Tomsick J. A., 2006, ApJ, 642, 438

Giacconi R., Murray S., Gursky H., Kellogg E., Schreier E., Matilsky T., Koch D., Tananbaum H., 1974, ApJS, 27, 37

Hakala P. J., Muhli P., Dubus G., 1999, MNRAS, 306, 701

Hakala P., Muhli P., Charles P., 2014, MNRAS, 444, 3802

Hjellming R. M., Rupen M. P., Mioduszewski A. J., 1998, IAU Circ., 6924, 1

Hynes R. I., Roche P., Charles P. A., Coe M. J., 1999, MNRAS, 305, L49

in 't Zand J., Heise J., Bazzano A., Cocchi M., di Ciolo L., Muller J. M., 1999, IAU Circ., 7119, 1

Itoh R. et al., 2017, PASJ, 69, 25

Jana A., Jaisawal G. K., Naik S., Kumari N., Chhotaray B., Altamirano D., Remillard R. A., Gendreau K. C., 2021, MNRAS, 504, 4793

Kawamuro T. et al., 2018, Astron. Telegram, 11399

Kennea J. A. et al., 2019, Astron. Telegram, 13257

Khargharia J., Froning C. S., Robinson E. L., 2010, ApJ, 716, 1105

Kimura M. et al., 2016, Nature, 529, 54

Kong A. K. H., 2018, Astron. Telegram, 11949

Kosenkov I. A., 2021a, DIPol-UF: Remote Control Software for DIPol-UF Polarimeter, Zenodo, https://doi.org/10.5281/zenodo.6338401

Kosenkov I. A., 2021b, Dipol2Red: Linear Polarization Data Reduction Pipeline for DIPol-2 and DIPol-UF Polarimeters, Zenodo, https://doi.org/10.5281/zenodo.5763989

Kosenkov I. A., 2021c, PhD thesis, University of Turku, Finland

Kosenkov I. A., Berdyugin A. V., Piirola V., Tsygankov S. S., Pallé E., Miles-Páez P. A., Poutanen J., 2017, MNRAS, 468, 4362

Kosenkov I. A. et al., 2020, MNRAS, 496, L96

Krimm H. A. et al., 2011, Astron. Telegram, 3138

Lipunov V. et al., 2015, Astron. Telegram, 8453

Littlefield C., 2018, Astron. Telegram, 11421

Loh A. et al., 2016, MNRAS, 462, L111

MacDonald R. K. D. et al., 2014, ApJ, 784, 2

Makino F., Wagner R. M., Starrfield S., Buie M. W., Bond H. E., Johnson J., Harrison T., Gehrz R. D., 1989, IAU Circ., 4786, 1

Mata Sánchez D., Muñoz-Darias T., Casares J., Corral-Santana J. M., Shahbaz T., 2015, MNRAS, 454, 2199

McClintock J. E., Horne K., Remillard R. A., 1995, ApJ, 442, 358

Mikolajewska J., Zdziarski A. A., Ziolkowski J., Torres M. A. P., Casares J., 2022, ApJ, 930, 9

Miller-Jones J. C. A., Jonker P. G., Dhawan V., Brisken W., Rupen M. P., Nelemans G., Gallo E., 2009, ApJ, 706, L230

Mirabel I. F., Dhawan V., Mignani R. P., Rodrigues I., Guglielmetti F., 2001, Nature, 413, 139

Negoro H. et al., 2019, Astron. Telegram, 13256

Nowak M. A., Wilms J., 1999, ApJ, 522, 476

Orosz J. A. et al., 2001, ApJ, 555, 489

Orosz J. A., Steiner J. F., McClintock J. E., Torres M. A. P., Remillard R. A., Bailyn C. D., Miller J. M., 2011, ApJ, 730, 75

Piirola V., 1973, A&A, 27, 383

Piirola V., 1975, Ann. Acad. Sci. Fennicae, 418, 1

Piirola V., Berdyugin A., Berdyugina S., 2014, in Ramsay S. K., McLean I. S., Takami H., eds, Proc. SPIE Conf. Ser. Vol. 9147, Ground-based and Airborne Instrumentation for Astronomy V. SPIE, Bellingham, p. 91478I

Piirola V. et al., 2020, A&A, 635, A46

Piirola V., Kosenkov I. A., Berdyugin A. V., Berdyugina S. V., Poutanen J., 2021, AJ, 161, 20

Pooley G. G., 2005, Astron. Telegram, 385

Poutanen J., Veledina A., 2014, Space Sci. Rev., 183, 61

Poutanen J. et al., 2022, Science, 375, 874

Remillard R. et al., 1998, IAU Circ., 6920, 1

Remillard R., Morgan E., Smith D., Smith E., 2000, IAU Circ., 7389, 2

Remillard R., Garcia M., Torres M. A. P., Steeghs D., 2005, Astron. Telegram, 384

Richter G. A., 1989, Inf. Bull. Var. Stars, 3362, 1

Rodriguez J. et al., 2015, A&A, 581, L9

Rupen M. P., Dhawan V., Mioduszewski A. J., 2005, Astron. Telegram, 387

Russell D. M., Shahbaz T., Lewis F., Gallo E., 2016, MNRAS, 463, 2680

Rybicki G. B., Lightman A. P., 1979, Radiative Processes in Astrophysics. John Wiley & Sons, Ltd, New York, USA

Salvesen G., Pokawanvit S., 2020, MNRAS, 495, 2179

Schultz J., Hakala P., Huovelin J., 2004, Baltic Astron., 13, 581

Shahbaz T., Dhillon V. S., Marsh T. R., Zurita C., Haswell C. A., Charles P. A., Hynes R. I., Casares J., 2003, MNRAS, 346, 1116

Shahbaz T., Russell D. M., Zurita C., Casares J., Corral-Santana J. M., Dhillon V. S., Marsh T. R., 2013, MNRAS, 434, 2696

Shahbaz T., Russell D. M., Covino S., Mooley K., Fender R. P., Rumsey C., 2016, MNRAS, 463, 1822

Simmons J. F. L., Stewart B. G., 1985, A&A, 142, 100

Sobolev V. V., 1963, A Treatise on Radiative Transfer. Van Nostrand, Princeton

Stiele H., Kong A. K. H., 2020, ApJ, 889, 142

Strader J., Aydi E., Sokolovsky K., Shishkovsky L., 2019, Astron. Telegram, 13260

Tanaka Y. T. et al., 2016, ApJ, 823, 35

Thompson A. R., Clark B. G., Wade C. M., Napier P. J., 1980, ApJS, 44, 151

Thorstensen J. R., 1987, ApJ, 312, 739

Tomsick J. A. et al., 2019, Astron. Telegram, 13270

Torres M. A. P., Callanan P. J., Garcia M. R., Zhao P., Laycock S., Kong A. K. H., 2004, ApJ, 612, 1026

Torres M. A. P., Casares J., Jiménez-Ibarra F., Álvarez-Hernández A., Muñoz-Darias T., Armas Padilla M., Jonker P. G., Heida M., 2020, ApJ, 893, L37

Udalski A., Kaluzny J., 1991, PASP, 103, 198

Uttley P., Casella P., 2014, Space Sci. Rev., 183, 453

Veledina A. et al., 2019, A&A, 623, A75

Wagner R. M., Foltz C. B., Shahbaz T., Casares J., Charles P. A., Starrfield S. G., Hewett P., 2001, ApJ, 556, 42

Wijnands R., Miller J. M., van der Klis M., 2002, MNRAS, 331, 60

Zhirkov K. et al., 2021, Astron. Telegram, 15014

Zurita C. et al., 2006, ApJ, 644, 432

Życki P. T., Done C., Smith D. A., 1999, MNRAS, 309, 561

This paper has been typeset from a TeX/LaTeX file prepared by the author.